Tribology International 97 (2016) 390–399

Contents lists available at ScienceDirect

Tribology International

journal homepage: www.elsevier.com/locate/triboint

The lubrication approximation of the friction force for the simulation of measured surfaces

Hugo M. Checo *, Alfredo Jaramillo, Roberto F. Ausas, Gustavo C. Buscaglia

Inst. Ciências Matemáticas e de Computação, Univ. São Paulo, 13560-970 São Carlos, Brazil

ARTICLE INFO

Article history:
Received 20 August 2015
Received in revised form
30 November 2015
Accepted 23 December 2015
Available online 13 January 2016

Keywords:
Hydrodynamic lubrication
Friction force
Measured-surface simulation
Mass-conservative model

ABSTRACT

Models of the friction force are assessed by direct comparison with two-dimensional Navier–Stokes results. A three-term formula obtained from asymptotic expansion provides a reasonable estimate of the hydrodynamic friction of rough runners even at sub-micron clearances.

Simulations of a measured honed surface are then reported using the conservative time-dependent Elrod–Adams model with spatial resolutions as fine as 0.25 μm per cell (4000 × 800 mesh). Mesh convergence of the numerical method is observed. Cell sizes between 0.5 μm and 1 μm appear as a reasonable compromise of accuracy and cost for the simulation of honed runners. The significance of each term of the friction formula is discussed, so as to assess the error involved in neglecting terms of the friction formula.

1. Introduction

Theoretical and numerical studies of lubricated devices often represent the contacting surfaces as smooth. While this approximation stands under some conditions, this is not the case when the film thickness is comparable to the roughness amplitude, as in heavily loaded journal bearings, seals, piston ring/cylinder liner contacts, among others. The introduction of surface roughness into lubrication models can be traced back to the stochastic model of Tzeng and Saibel [1]. In their work, a probability distribution is adopted for the surface roughness and formulas of the expected values of pressure, friction force and load-carrying capacity are deduced for a one-dimensional problem. A more encompassing model was given by Christensen [2], who presented a modified (stochastic) Reynolds equation in which the coefficients were expected values. These results were limited to transverse or longitudinally oriented variations in roughness.

Later, Patir and Cheng [3,4] introduced a new approach. An average Reynolds equation for rough surfaces was defined in terms of pressure and shear flow factors, which were empirical functions of the non-dimensional roughness. Elrod [5] later extended this model to account for roughness anisotropy.

All of these techniques are based on the intuitive idea of decoupling the global length scale, corresponding to the whole bearing, from the local length scale of the roughness. Homogenization theory formalizes this intuition. It develops an average equation valid throughout the domain, with its coefficients computed from solutions of local problems. The homogenization method has been studied in depth both for incompressible [6,7] and compressible [8–10] fluids. It exhibits good accuracy when the roughness is periodic in space and its period is much smaller than the bearing size. Unfortunately, no rigorous homogenization model considers general roughness shapes with cavitation effects.

A current trend is to study the hydrodynamics of lubrication devices resolving all scales of the problem down to the roughness scale, using the measured topography and without resorting to averaged or stochastic models. These so-called *deterministic* or *measured-surface* simulations [11–14] avoid ambiguities in the definition of average coefficients at the expense of solving Reynolds equation with a discretization finer than the resolution of the measurements. A central result of the simulations is the hydrodynamic force exerted by the fluid, defined by

$$\mathbf{F} = \int_S \boldsymbol{\sigma} \cdot \check{\mathbf{n}}\, dS, \tag{1}$$

of which the component parallel to the movement is the *friction force*. Different formulae for the lubrication approximation of Eq. (1) appear in the literature. Patir and Cheng [4] identify the existence of three terms in this approximation, which we denote here as Couette term F^{cou}, Poiseuille term F^{poi} and pressure term F^{pre},

* Corresponding author. Tel.: + 55 16 9233 3043.
E-mail addresses: hugocheco@gmail.com (H.M. Checo), ajaramillopalma@gmail.com (A. Jaramillo), rfausas@gmail.com (R.F. Ausas), gustavo.buscaglia@gmail.com (G.C. Buscaglia).

http://dx.doi.org/10.1016/j.triboint.2015.12.030
0301-679X/

the first two being shear forces, while the latter is the projection of the pressure force on the surface along the movement direction. While some authors consider all three terms [15–17], there exist publications in which only F^{cou} is considered (thus not requiring knowledge of the pressure [18–22]) and others in which F^{pre} is neglected [23,24], i.e., just considering the shear stresses.

This paper, after the necessary definitions, introduces the complete three-term formula from a formal asymptotic expansion in Section 2. Its accuracy is confirmed in Section 3 by performing a direct comparison against Navier–Stokes results. Section 4 then contains deterministic simulations with measured data from a honed surface representative of automotive cylinder liners. To our knowledge, these are the first mesh-converged simulations that consider the unsteadiness that results from the motion of the rough surface through the computational domain. It is shown that all three terms in the friction formula are significant for clearances below 1 or 2 microns, both for conformal and non-conformal contacts. Further discussions and the conclusions are left for Section 5.

2. Model

2.1. Hydrodynamic lubrication model

We consider two surfaces in close proximity and in relative motion with velocity V. The upper surface is assumed rigid, its elevation with respect to the (reference) plane x_1-x_2 being given by a known function $h_U(x_1,x_2)$ (Fig. 1). The lower surface, also considered rigid, moves along the axis x_1. If its elevation at time $t=0$ is given by the function $h_L(x_1,x_2)$, also known, then the gap between the surfaces is

$$h(x_1,x_2,t)=h_U(x_1,x_2)-h_L(x_1-V\,t,x_2). \tag{2}$$

To model starvation and cavitation effects, the lubricating fluid is assumed to fill a fraction $\theta(x_1,x_2,t)$ of the gap $h(x_1,x_2,t)$. In this situation, and most especially if the gap thickness h exhibits small-scale features, it is important to adopt a mass-conserving model [25]. We use here the Elrod–Adams model [26], which incorporates into a single formulation the Reynolds equation and the Jacobsson–Floberg–Olsson boundary conditions. Two scalar fields must be solved at every point of the domain: the hydrodynamic pressure $p=p(x_1,x_2,t)$ and the saturation $\theta=\theta(x_1,x_2,t)$. The governing equation reads

$$\nabla\cdot\left(\frac{h^3}{12\mu}\nabla p\right)=\frac{V}{2}\frac{\partial\, h\theta}{\partial x_1}+\frac{\partial\, h\theta}{\partial t}\quad\text{in}\quad \Omega=\{[x_{1\ell},x_{1r}]\times[0,B]\}, \tag{3}$$

where μ is the viscosity and Ω the simulation domain. Eq. (3) must hold under the pointwise complementarity conditions on p and θ

$$\begin{cases} p>0 & \Rightarrow \quad \theta=1\\ \theta<1 & \Rightarrow \quad p=0\,.\\ 0\le\theta\le 1 & \end{cases} \tag{4}$$

The Elrod–Adams model, from which the classical Reynolds equation is recovered by taking $\theta\equiv 1$, can be justified physically under the so-called *lubrication hypotheses* [27], i.e.,

$$\frac{h}{\ell}\ll 1,\quad \|\nabla h\|\ll 1, \tag{5}$$

where ℓ is a length scale of the problem in the x_1-x_2 plane.

2.2. Lubrication approximation of the friction force

The total force exerted by an incompressible Newtonian fluid on a surface S is given by

$$\mathbf{F}=\int_S \boldsymbol{\sigma}\cdot\check{\mathbf{n}}\,dS=\int_S\left[-p\mathbb{I}+\mu\left(\nabla\mathbf{u}+\nabla\mathbf{u}^T\right)\right]\cdot\check{\mathbf{n}}\,dS, \tag{6}$$

where $\mathbb{I}$ is the identity matrix, $\mathbf{u}=(u_1,u_2,u_3)$ is the velocity field of the fluid and $\nabla\mathbf{u}$ its gradient, and $\check{\mathbf{n}}$ is the inward normal. The component of $\mathbf{F}$ along the direction of motion (i.e., the first component) is the *friction force* F. Computing F on the lower surface, since the normal is given by

$$\check{\mathbf{n}}=\frac{(-\partial h_L/\partial x_1,\,-\partial h_L/\partial x_2,\,1)}{\sqrt{1+\left(\partial h_L/\partial x_1\right)^2+\left(\partial h_L/\partial x_2\right)^2}}, \tag{7}$$

one gets

$$F_L=\int_\Omega\left[-\frac{\partial h_L}{\partial x_1}\left(-p+2\mu\frac{\partial u_1}{\partial x_1}\right)-\frac{\partial h_L}{\partial x_2}\mu\left(\frac{\partial u_1}{\partial x_2}+\frac{\partial u_2}{\partial x_1}\right)+\mu\left(\frac{\partial u_1}{\partial x_3}+\frac{\partial u_3}{\partial x_1}\right)\right]dx_1dx_2. \tag{8}$$

Let us now consider a change of variables $z=x_3/\epsilon$, where ϵ is arbitrarily small. As done in [28], assume that p and $\mathbf{u}$ can be written as a power series in ϵ:

$$\mathbf{u}=\mathbf{u}^{(0)}+\epsilon\mathbf{u}^{(1)}+\epsilon^2\mathbf{u}^{(2)}+\cdots \tag{9a}$$

$$p=\frac{1}{\epsilon^2}p^{(0)}+\frac{1}{\epsilon}p^{(1)}+p^{(2)}+\cdots. \tag{9b}$$

Substitution into Eq. (8) produces

$$F_L=\int_\Omega\left[\epsilon^{-1}\left(p^{(0)}\frac{\partial h_L}{\partial x_1}+\mu\frac{\partial u_1^{(0)}}{\partial z}\right)+\epsilon^0\left(p^{(1)}\frac{\partial h_L}{\partial x_1}+\mu\frac{\partial u_1^{(1)}}{\partial z}\right)+\epsilon(\ldots)+\cdots\right]dx_1dx_2. \tag{10}$$

Knowing that $u_1^{(0)}$ satisfies [28]

$$u_1^{(0)}=\frac{1}{2\mu}\frac{\partial p^{(0)}}{\partial x_1}z(z-h)+\left(1-\frac{z}{h}\right)V \tag{11}$$

and going back to the original variable x_3, Eq. (10) becomes

$$F_L=\int_\Omega\left[\left(-\frac{\mu V}{h}-\frac{1}{2}h\frac{\partial p^{(0)}}{\partial x_1}+p^{(0)}\frac{\partial h_L}{\partial x_1}\right)+\epsilon\left(p^{(1)}\frac{\partial h_L}{\partial x_1}+\mu\frac{\partial u_1^{(1)}}{\partial x_3}\right)+\epsilon^2(\ldots)+\cdots\right]dx_1dx_2. \tag{12}$$

The leading order asymptotic approximation of the friction force as computed on the lower surface is thus given by

$$F_L(t)\simeq-\int_\Omega\left(\frac{\mu V}{h}+\frac{1}{2}h\frac{\partial p}{\partial x_1}-p\frac{\partial h_L}{\partial x_1}\right)dx_1dx_2. \tag{13}$$

Similarly, for the upper surface,

$$F_U(t)\simeq-\int_\Omega\left(-\frac{\mu V}{h}+\frac{1}{2}h\frac{\partial p}{\partial x_1}+p\frac{\partial h_U}{\partial x_1}\right)dx_1dx_2. \tag{14}$$

The previous approximations, having started from Eq. (6) and thus considering a single-phase incompressible fluid between the surfaces, do not consider cavitation effects. Friction models in cavitated areas are controversial. We adopt here a slight modification of the formulas above, in which the first term is multiplied by a heuristic factor $g(\theta)$, which in this work we take as

$$g(\theta)=\begin{cases}\theta & \text{if } \theta>\theta_s=0.95\\ 0 & \text{otherwise.}\end{cases} \tag{15}$$

The parameter θ_s is a threshold for the onset of friction, which can be interpreted as the minimum oil fraction for shear forces to be transmitted from one surface to the other. The results are not qualitatively sensitive to θ_s, as reported in [15]. The other two terms are left unmodified, and thus are equal to zero in the cavitated region. The final heuristically modified model arising from

the asymptotic expansion reads

$$F_L(t) = -\int_\Omega \left(\mu\frac{Vg(\theta)}{h}+\frac{1}{2}h\frac{\partial p}{\partial x_1}-p\frac{\partial h_L}{\partial x_1}\right)dx_1dx_2, \tag{16a}$$

$$F_U(t) = -\int_\Omega \left(-\mu\frac{Vg(\theta)}{h}+\frac{1}{2}h\frac{\partial p}{\partial x_1}+p\frac{\partial h_U}{\partial x_1}\right)dx_1dx_2. \tag{16b}$$

Three terms are identified in the previous equations. For the lower surface they are the Couette term:

$$F_L^{cou}(t) = -\int_\Omega \left(\mu\frac{Vg(\theta)}{h}\right)dx_1\,dx_2, \tag{17}$$

the Poiseuille term

$$F_L^{poi}(t) = -\int_\Omega \left(\frac{1}{2}h\frac{\partial p}{\partial x_1}\right)dx_1\,dx_2, \tag{18}$$

and the pressure term

$$F_L^{pre}(t) = \int_\Omega \left(p\frac{\partial h_L}{\partial x_1}\right)dx_1\,dx_2. \tag{19}$$

We consider three models for the friction force. The first model is the one obtained from the asymptotic expansion:

$$F_L^I = F_L^{cou}+F_L^{poi}+F_L^{pre}. \tag{20}$$

The second one [23,24],

$$F_L^{II} = F_L^{cou}+F_L^{poi}, \tag{21}$$

neglects the normal contribution of the pressure, while the third model [18–22],

$$F_L^{III} = F_L^{cou}, \tag{22}$$

computes the friction force with just the Couette term. Analogous definitions can be made for $F_U{}^I$, $F_U{}^{II}$ and $F_U{}^{III}$.

It is to be noticed that only models F^I and F^{III} satisfy that the forces on the upper and lower surfaces add up to zero. For model F^{III} this is obvious, while for model F^I it is verified as follows:

$$F_L^I(t)+F_U^I(t) = -\int_{\Omega^+}\left(h\frac{\partial p}{\partial x_1}-p\frac{\partial h_L}{\partial x_1}+p\frac{\partial h_U}{\partial x_1}\right)d\Omega \tag{23}$$

$$= -\int_{\Omega^+}\left(h\frac{\partial p}{\partial x_1}+p\frac{\partial (h_U-h_L)}{\partial x_1}\right)d\Omega \tag{24}$$

$$= -\int_{\Omega^+}\left(h\frac{\partial p}{\partial x_1}+p\frac{\partial h}{\partial x_1}\right)d\Omega \tag{25}$$

$$= -\int_{\Omega^+}\frac{\partial (ph)}{\partial x_1}d\Omega = -\int_{\partial\Omega^+} ph\check{\mathbf{n}}\cdot\check{\mathbf{e}}_1 d\Gamma = 0, \tag{26}$$

where Ω^+ is the region where $p>0$ and $\partial\Omega^+$ its boundary.

2.3. Numerical method

The conservative finite volume method described in [29] is used to solve problem (3)–(4). The complementarity conditions are imposed iteratively in a Gauss–Seidel-type algorithm. Computational times are alleviated through multigrid acceleration [30,11]. This method has been validated against semi-analytic solutions and used in technological applications such as journal bearings and the piston-ring/liner contact [25,29,15,16].

3. Assessment of friction force formulae against single-phase Navier-Stokes simulations

In the previous section, we have presented three models for the calculation of the friction force from the results (p and θ) of the Elrod–Adams model. The first one, denoted by F^I, was obtained from an asymptotic expansion, while the other two (F^{II} and F^{III}) omit terms that appear in F^I and have been taken from the literature. In this section, we assess the accuracy of the three models against accurate numerical solutions of the incompressible Navier–Stokes equations. Similar assessments have been reported previously [31,32], though not addressing the friction calculation. A remark must be made here: the comparison presented in this section neglects both inertia and cavitation effects. Neglecting cavitation implies $\theta\equiv 1$, so that the Elrod–Adams result is, in fact, the solution of the Reynolds equation. To deal with the cavitation issue more sophisticated CFD simulations involving moving boundaries and phase change would be necessary.

To further simplify the comparison, we consider all variables independent of x_2 and solve the flow at the single instant $t=0$ in the two-dimensional domain:

$$\{(x_1,x_3)\,|\,0\le x_1\le\lambda,\quad h_L(x_1)\le x_3\le h_U(x_1)\}, \tag{27}$$

using a finite element in-house code which has been extensively validated (see [33–35]). The unknowns are the velocity field $\mathbf{u}_h$ and the pressure field p_h. The boundary conditions are: (a) $\mathbf{u}_h=(0,0)$ on the upper surface. (b) $\mathbf{u}_h=(V,0)$ on the lower surface. (c) periodic boundary conditions at $x_1=0$ and $x_1=\lambda$. The pressure is thus determined up to an additive constant, which has no effect on the value of the friction force. Once $\mathbf{u}_h$ and p_h have been solved for, a nodal approximation of

$$\boldsymbol{\sigma}_h = -p_h\,\mathbb{I}+\mu\left(\nabla\mathbf{u}_h+\nabla\mathbf{u}_h^T\right) \tag{28}$$

is built. The friction force on a surface S is then computed from

$$F^{NS} = \int_S(\boldsymbol{\sigma}_h\cdot\check{\mathbf{n}})\cdot\check{\mathbf{e}}_1\,dS \tag{29}$$

assuming $\boldsymbol{\sigma}_h$ independent of x_2. Above, $\check{\mathbf{e}}_1$ denotes the horizontal unit vector $(1,0,0)$. In all simulations, it was checked that mesh

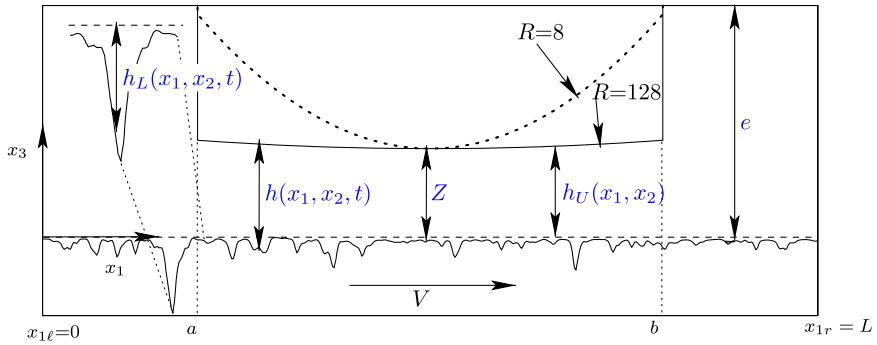

Fig. 1. A cross-section of the domain showing the geometrical parameters of the problem.

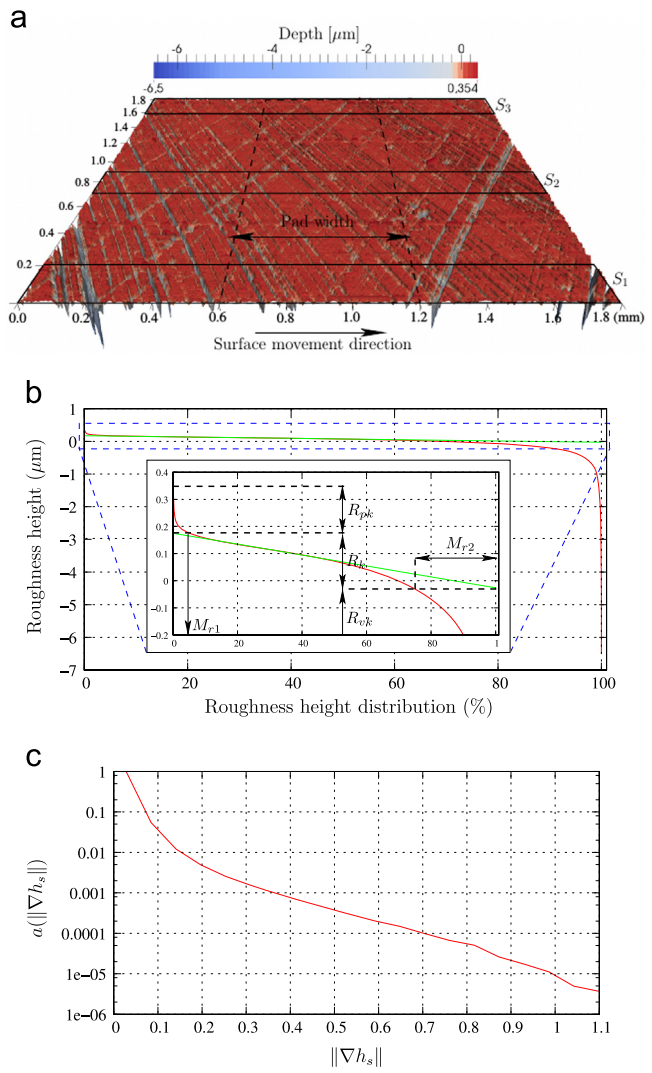

Fig. 2. (a) View of the honed measured surface with depth in micrometers. (b) Abbott–Firestone curve for the surface shown in Fig. (a) and (b) fractional distribution $a(\cdot)$ of the measured surface according to the norm of its gradient $\|\nabla h_s\|$.

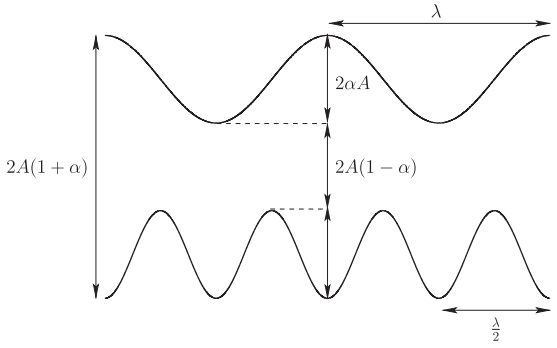

Fig. 3. Scheme of the geometrical setting to compare Reynolds and Navier–Stokes results.

convergence of the Navier–Stokes solver had been attained, with discretization error not larger than 1% in all relevant variables.

The numerical experiments consider sinusoidal profiles for both the upper and lower surfaces:

$$h_U(x_1) = A[1+\alpha\,\cos(2\,\pi x_1/\lambda)], \quad h_L(x_1) = -A[1+\alpha\,\cos(4\,\pi x_1/\lambda)] \tag{30}$$

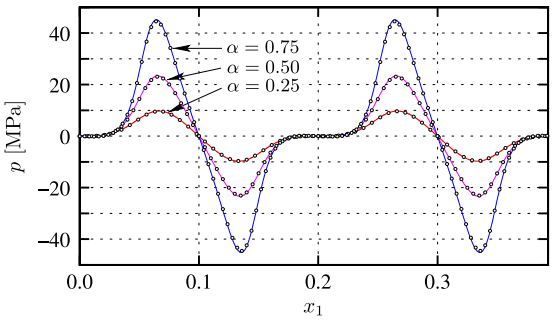

Fig. 4. Comparison of the pressure profiles for different values of the relative waviness amplitude α as obtained by numerically solving the Reynolds equation (continuous lines) and the Navier–Stokes equations (circles). In the latter case, the pressure profile corresponds to $x_3 = 0$.

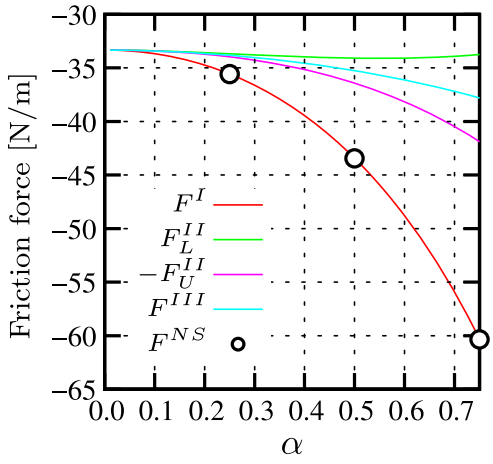

Fig. 5. Total horizontal force as a function of the relative waviness amplitude α. The Navier–Stokes reference values F^{NS} are plotted with circles (for $\alpha = 0.25$, 0.5 and 0.75), and they are seen to coincide with the results of the first model F^I. The other two models fail to reproduce the dependence of the friction force with α.

where $2A$ is the mean distance between the surfaces and αA the waviness amplitude for both surfaces. The wavelength in the upper surface is λ, while that of the lower surface is $\lambda/2$. A scheme of the geometrical setting is shown in Fig. 3.

The simulations consider $A = 0.3$ μm, $\lambda = 200$ μm, and several values of α between 10^{-3} and 0.75. From the definitions of Eq. (30) one observes that

$$\frac{h_{\max}}{\lambda} = \frac{2(1+\alpha)A}{\lambda} \quad \text{and} \quad \|\nabla h\|_{\max} = \frac{17.2\,\alpha\,A}{\lambda}.$$

For our values $A/\lambda = 1.5 \times 10^{-3}$, so that conditions (5) are satisfied and good agreement between the Navier–Stokes solution and the Reynolds solution is expected.

The Navier–Stokes solver was run on a very fine mesh consisting of 160,000 linear triangular elements. Its results were compared with those of the Reynolds solver run on a mesh of 2000 one-dimensional cells. Fig. 4 shows that both models predict exactly the same pressure field.

Let us now compare the three friction models F^I, F^{II} and F^{III}, as computed from the Reynolds pressure solution, with the force F^{NS} obtained from the Navier–Stokes solution. This is plotted in Fig. 5. One observes that model F^I agrees with F^{NS} in the whole range of the relative amplitude α. The other two models, though coincident with F^{NS} when $\alpha = 0$ (parallel bearing), completely fail to reproduce the dependence of the friction force with α.

In simulations of measured surfaces, however, the lubrication hypotheses (5) are close to their limit of validity, specially the second one. Fig. 2 illustrates a specific topography, corresponding

to a honed cylinder, which is an example of the kind of measured data for the function h_L. Part (c) of the figure shows the fractional distribution $a(\|\nabla h_L\|)$ on the surface. For any number s, the value $a(s)$ is the fraction of the surface which has $\|\nabla h_L\| > s$. The gradient is computed by discrete differentiation of the matrix of measured points. By direct inspection of Fig. 2(c), one observes that there are points where the hypothesis $\|\nabla h_L\| \ll 1$ is not satisfied.

It is thus also interesting to use our two-dimensional toy example to evaluate the accuracy of lubrication models against Navier–Stokes predictions for values of $\|\nabla h_L\|$ of order unity, focusing on the accuracy of friction predictions.

Fixing $A=0.3\,\mu$m and $\alpha=0.75$, simulations with smaller values of λ were performed, as shown in Table 1. For $\lambda=2\,\mu$m the maximum $\|\nabla h_L\|$ is 1.935, in clear violation of Eq. (5) and one observes that all lubrication friction formulas provide poor predictions. The pressure and velocity fields produced by the Navier–Stokes solver are shown in Fig. 6. Vertical gradients of the pressure field are evident, a clear sign that the lubrication approximation does not hold. For $\lambda \geq 10\,\mu$m, which corresponds to $\|\nabla h_L\|_{\max} \leq 0.387$, Table 1 shows that the lubrication approximation with friction model F^I predicts the reference value F^{NS} with good accuracy, while models F^{II} and F^{III} fail.

Table 1
Comparison of the friction lubrication models F_L^I, F_L^{II} and F_L^{III} with the Navier–Stokes result F_L^{NS} for short waviness wavelengths. For all cases $\mu=0.01$ Pa-s, $V=10$ m/s, $A=300\,\mu$m and $\alpha=0.75$. The second column is $\max_{x_1}|\partial h/\partial x_1|$. The friction force per unit width (along x_2), integrated over one wavelength λ in x_1, is given in Newton/meter. Between parentheses the relative error of each model as compared to F_L^{NS}. Analogous results are obtained if the integration is performed on the upper surface.

λ (μm)	$\|\nabla h\|_{\max}$	F_L^{NS}	F_L^I	F_L^{II}	F_L^{III}
2	1.935	−0.890	−0.603 (32%)	−0.337 (62%)	−0.378 (57%)
10	0.387	−3.198	−3.016 (5.7%)	−1.687 (47%)	−1.891 (41%)
20	0.193	−6.148	−6.032 (1.9%)	−3.374 (45%)	−3.782 (38%)
200	0.019	−60.36	−60.32 (<0.1%)	−33.74 (44%)	−37.81 (37%)

On the basis of these results, we conclude that the friction force model F^I, which can be obtained from an asymptotic expansion, is the best formula for approximating the friction force in lubrication models based on the Reynolds equation. This model, which consists of three terms (Couette, Poiseuille and Pressure terms), exhibits good accuracy when applied to surfaces with characteristics similar to those of honed surfaces and will be considered hereafter as *correct*. In the following section, we solve the Elrod–Adams model using the measured honed surface data so as to estimate the importance of each term in the friction formula under realistic conditions.

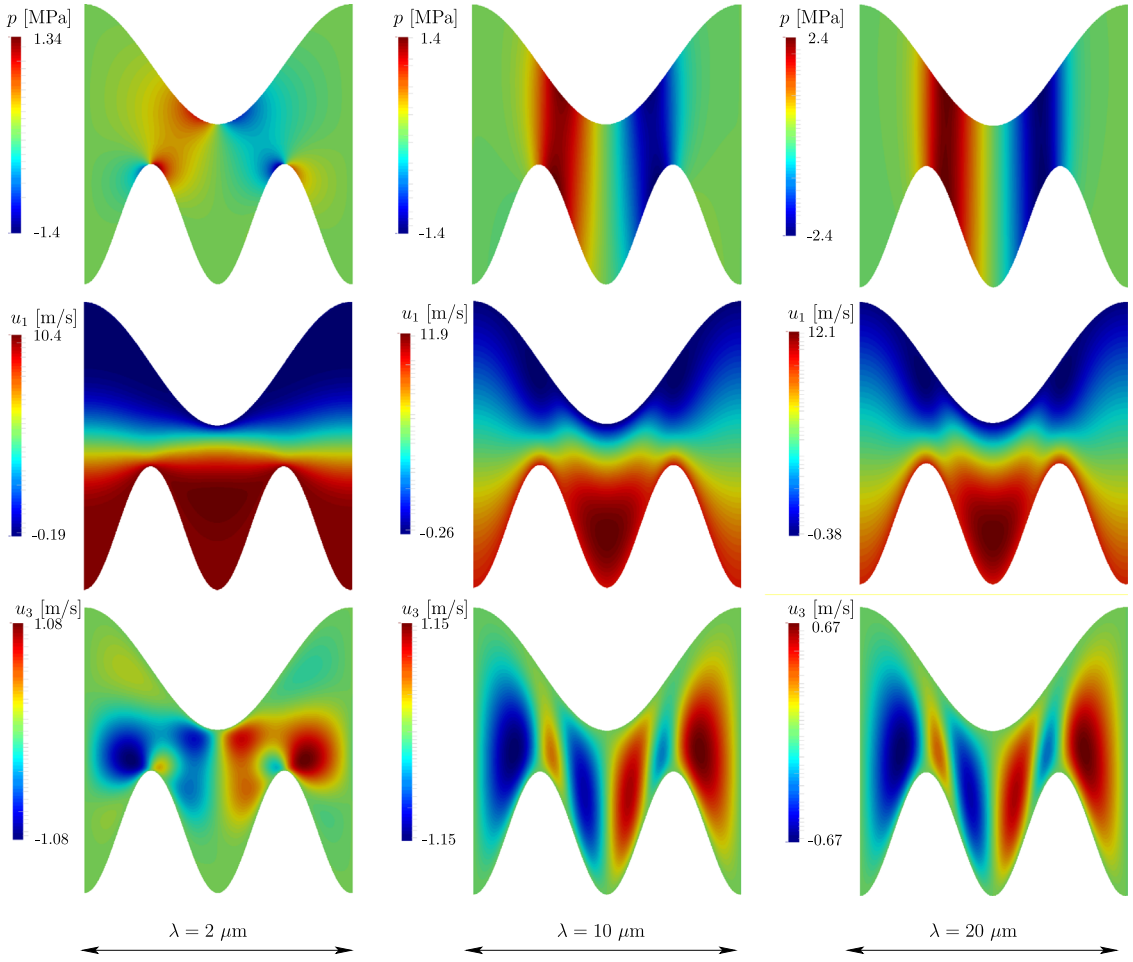

Fig. 6. Contours of pressure (p, top line) and velocity components (u_1, u_3, middle and bottom lines) corresponding to the Navier–Stokes simulations with $\lambda=2$ (left column), 10 (center column) and 20 μm (right column).

Table 2
Surface-finish parameters for the surface of Fig. 2(a).

Parameter	Value
S_a	0.15 μm
S_q	0.25 μm
S_{sk}	−6.56
S_{ku}	81.8
R_{pk}	0.18 μm
R_k	0.2 μm
R_{vk}	6.47 μm
M_{r1}	6.6%
M_{r2}	24.1%

4. Numerical simulations of measured honed surfaces

We consider as upper surface a single barrel-shaped pad, inspired in the shape of compression piston rings of car engines. Its shape corresponds to an arc of circumference of radius R. Its height h_U with respect to the reference plane is:

$$h_U(x_1,x_2)=\begin{cases} Z+R-\sqrt{R^2-\left(x_1-\frac{L}{2}\right)^2} & \text{if } a\le x_1\le b \\ e & \text{otherwise} \end{cases} \tag{31}$$

The parameter Z is the minimal distance between the surface and the x_1-x_2 plane and e is a constant much larger than Z. This pad slides with constant velocity $-V$ over the measured topography of a cross-hatched finished plane (honed runner). This finish is typical of cylinder liners of car engines. The measured surface is the one shown in Fig. 2(a). A proper way to characterize a honed surface is by means of its Abbott–Firestone curve [36]. This is given in Fig. 2(b) for the surface under study. Its related roughness parameters R_k (plateau height), R_{pk} (reduced peak height), R_{vk} (reduced valley height), M_{r1} (percentage of R_{pk} peaks) and M_{r2} (percentage of R_{vk} valleys) are shown in Table 2, along with the more conventional parameters S_a (roughness average), S_q (root mean square roughness), S_{sk} (skewness) and S_{ku} (kurtosis).

The measured surface dimensions are $L_s\times L_s$ with $L_s=1.8$ mm, sampled each 2 μm in both directions. In order to decrease the computational effort, instead of solving the problem on the whole surface, it is solved on three strips S_1, S_2 and S_3 of width $B=0.2$ mm, as indicated in the same figure. The measured points provide a function $x_3=h_s(x_1,x_2)$. The reference plane (x_1-x_2) is defined as the average height of the measured points, so that

$$\int_0^{L_s}\int_0^{B} h_s(x_1,x_2)\,dx_1\,dx_2=0. \tag{32}$$

The domain of this function along x_1 is just the interval $[0,L_s]$, which is too small to conduct simulations. We extended it periodically to tackle this difficulty. Incorporating also the movement of the runner with respect to the simulation frame of reference (fixed to the pad) one gets the function $h_L(x_1,x_2,t)$ as follows: Let n be an integer (negative in general) such that $2nL_s\le x_1-Vt<2(n+1)L_s$, then

$$h_L(x_1,x_2,t)=\begin{cases} h_s(x_1-Vt-2nL_s,x_2) & \text{if } 0\le x_1-Vt-2nL_s<L_s \\ h_s(2L_s-(x_1-Vt-2nL_s),x_2) & \text{if } L_s\le x_1-Vt-2nL_s\le 2L_s \end{cases}. \tag{33}$$

The resulting function h_L is depicted at the top of Fig. 7, in which the sector covered by the computational domain at time $t=1.6\times10^{-4}$ s is indicated. The remaining physical parameters defining the domain size, pad dimensions, fluid viscosity and surface velocity are given in Table 3. Reflection boundary conditions (corresponding to zero normal derivative of the pressure) are imposed at $x_2=0$ and $x_2=B$. A constant film height d is assumed at the entrance, which amounts to enforce $\theta=d/h$ at $x_1=x_{1\ell}$. The chosen d value ensured fully-flooded conditions for all the simulations performed. The pressure at $x_1=0$ is zero, since the film is incomplete, while outflow boundary conditions are set at $x_1=L$.

4.1. Mesh convergence study

The complex topography of the runner surface compels the use of a fine mesh, but it is unclear how fine it should be as compared to the spacing of the measured points (which is 2 μm in our case). A mesh convergence study is reported here to determine the level of discretization required to decrease the error in the solution to acceptable levels.

The study was performed on the strip S_1 with parameters $Z=2$ μm and $R=128$ mm. A typical snapshot of the solution is shown in Fig. 7. Part (a) shows the pressure over the computational domain, while part (b) shows a cross-section along $x_2=B/2$. Parts (c) and (d) show the saturation field θ, in which regions with $\theta<1$ identify cavitated zones. Finally, parts (e) and (f) show the friction force density f, defined as

$$f=\mu\frac{V}{h}g(\theta)+\frac{1}{2}h\frac{\partial p}{\partial x_1}-p\frac{\partial h_L}{\partial x_1}, \tag{34}$$

which is observed to be highly oscillatory in both space and time.

The computational domain Ω was discretized using 500×100, 1000×200, 2000×400 and 4000×800 finite volumes. This corresponds to $\Delta x_1=\Delta x_2=2$, 1, 0.5 and 0.25 μm, respectively. A recent measured surface simulation by Bouassida [11] used $\Delta x_1=\Delta x_2=0.78$ μm and a mesh of 1400×512 cells. The time step was taken such that the Courant number $C=(V/2)(\Delta t/\Delta x_1)$ equals unity for all meshes, that is $\Delta t=0.4$, 0.2, 0.1 and 0.05 μs corresponding to 1500, 3000, 6000 and 12,000 time steps for each mesh, respectively.

Convergence was numerically verified for all variables. Fig. 8 (a) and (b) show the hydrodynamic lift,

$$L(t)=\int_a^b\int_0^B p(x_1,x_2,t)\,dx_1\,dx_2, \tag{35}$$

and the friction force $F_L^I(t)$ as functions of time for the four meshes. Clearly, the difference between the two finest meshes is negligible for practical purposes.

Part (c) of the figure contains a cross-section of p along $x_2=B/2$ at an arbitrary instant ($t=1$), showing that pointwise convergence is also (almost) verified with the same refinement.

This study suggests that the 2000×400 mesh, with mesh spacing taken as one fourth of the measurement spacing, is practically converged and correctly represents the exact solution between the pad and the measured topography. This mesh is thus adopted in all results that follow.

4.2. Term-by-term contribution to friction

Results were obtained for the three strips S_1, S_2 and S_3, two different curvature radii $R=8$ and 128 mm, and for four separations between the pad and the runner: $Z=0.5$, 1.0, 2.0 and 4.0 μm, totaling 24 runs of the code. Each run takes about 3.0 h on a six-cored Intel i7-4930 K desktop computer with a 3.4 GHz clock rate. In the simulated conditions there is no contact between the surfaces, since $\min_{(x_1,x_2)\in\Omega}h(x_1,x_2,t)=0.13$ μm for all t.

The relative contribution of each of the three terms of the friction force (model F_L^I) are calculated as

$$\frac{F_L^{cou}(t)}{F_L^I(t)},\quad \frac{F_L^{poi}(t)}{F_L^I(t)}\quad\text{and}\quad \frac{F_L^{pre}(t)}{F_L^I(t)}. \tag{36}$$

Notice that the sign of each term is kept, so that though the relative contributions add up to one the individual terms can take any sign. They are shown as functions of time for strip S_1 in Fig. 9.

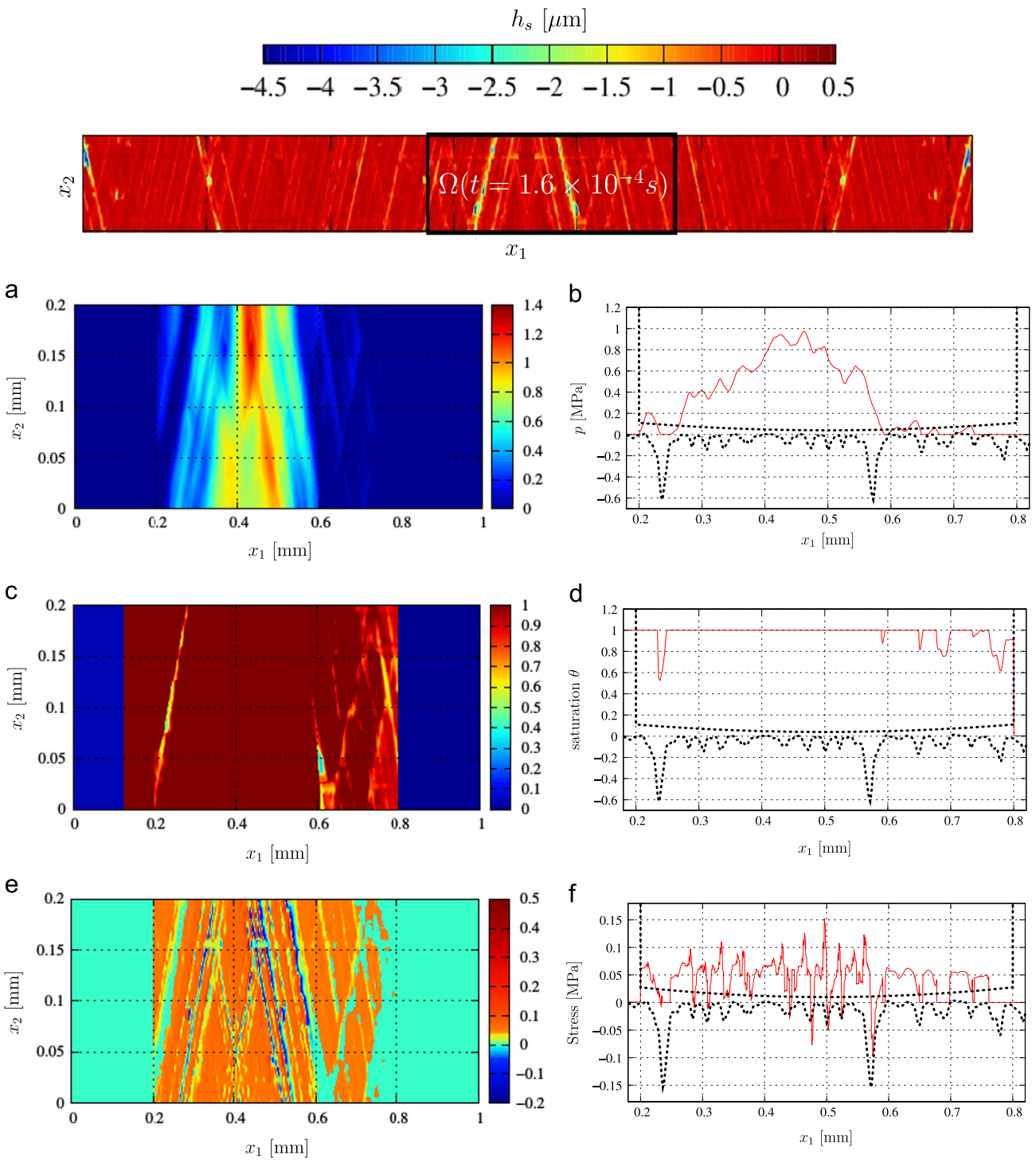

Fig. 7. Fields (a) p, (c) θ and (e) f at $t = 1.6 \times 10^{-4}$ s for strip S_1. This solution corresponds to parameters Z=2.0 and R=128. The right column shows cross-sections of the fields along $x_2 = B/2$.

Parts (a) and (b) correspond to the Couette term for R=8 and 128 mm, respectively. The general trend is that the Couette term becomes increasingly dominant as Z is increased, and also less oscillatory in time due to the higher average clearance. For the higher curvature pad, R=8 mm, the time-averaged contribution of the Couette term is 68% for Z=0.5 μm, growing to 89% for Z=4 μm. For the lower curvature pad, R=128 μm, it is 89% for Z=0.5 μm and 99% for Z=4 μm.

Parts (c) and (d) of Fig. 9 correspond to the Poiseuille term. Its contribution to the total friction force diminishes as Z increases, opposite to the trend seen with the Couette term. This term's relative contribution changes significantly with time at low Z. Interestingly, it is positive for the higher curvature pad and negative for the lower curvature one, which can be considered a conformal contact. For the rough surface chosen for this study, the Poiseuille term is thus seen to compensate to some extent the Couette term in conformal contacts at low clearance, reducing the friction force computed by the model.

The pressure term, on the other hand, is mostly positive (see parts (e) and (f) of the figure), as explained in [15]. Furthermore, it

Table 3
Physical parameters defining the problem.

Parameter	Value	Units	Description
μ	0.01	Pa.s	Fluid viscosity
a	0.2	mm	Leftmost position of pad in x_1
b	0.8	mm	Rightmost position of pad in x_1
d	20	μm	Fluid film height at the entrance $x_1 = x_{1\ell}$
e	500	μm	Clearance for $x_1 < a$ and $x_1 > b$
V	10	m/s	Sliding velocity
$x_{1\ell}$	0	mm	Left boundary of computational domain
x_{1r}	1.0	mm	Right boundary of computational domain
B	0.2	mm	Width of computational domain
L	1.0	mm	Length of computational domain
R	8, 128	mm	Radii of pad
Z	0.5, 1.0, 2.0, 4.0	μm	Distance from pad to the reference plane $x_1 - x_2$

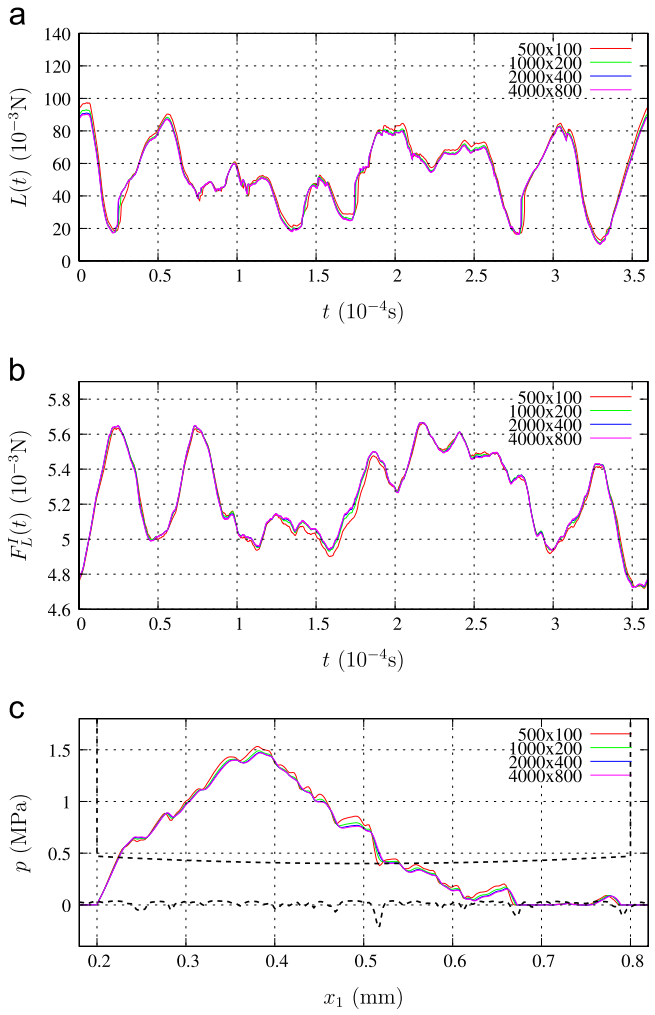

Fig. 8. (a) Hydrodynamic lift, (b) friction force, and (c) pressure at $t=1.0$ in $x_2=0.1$ computed with the four meshes of the convergence study.

is consistently larger than the Poiseuille term for the low curvature pad, at all values of Z, while for the $R=8$ pad it is much smaller. The net effect of $F_L^{poi}+F_L^{pre}$ is a *positive* contribution to the friction, which can be confirmed by noticing that the curves of F_L^{cou}/F_L^I never exceed unity. Results of the term-by-term analysis of strips S_2 and S_3 showed the same general trends as S_1.

From the relative contribution of each term one can quantify the error resulting from adopting models F^{II} or F^{III}:

$$e^{II} = \frac{F^{II} - F^I}{F^I}, \tag{37a}$$

$$e^{III} = \frac{F^{III} - F^I}{F^I}. \tag{37b}$$

The average values of these errors for the twenty-four conditions considered are shown in Table 4. Results for the three strips are quite similar.

The error of F^{II} for the results computed with $R=8$ (first column) are the lowest in the table, which can be explained by the small pressure terms, as seen in Fig. 9(e). The second lowest are the F^{III} errors for the results computed with $R=128$ (last column). This can be explained by: (a) the aforementioned cancellation of the Poiseuille and pressure terms for $R=128$ and (b) lower average Poiseuille and pressure terms (Fig. 9(d) and (f)) at low Z values. For the same model, the errors computed for $R=8$ are the largest in the table. While the pressure term drops rapidly with Z (Fig. 9(e)) the Poiseuille term remains relatively high (approximately 10% for $Z=4.0$), thus making e^{III} of about the same order as the Poiseuille term for high Z values.

The error e^{II} represents the omission of the pressure term in F^I. The contribution of the pressure term decreases with increasing Z, the errors are below 4% and also comparable in size for both R values and $Z \geq 2.0$. Larger errors are observed for lower Z values.

In general, omitting terms in the friction force has a significant impact on friction evaluation, especially at low clearances. For $Z=0.5$ the errors are of about 10% or as large as 30%.

If Z is large enough compared with the surface's roughness, it is expected that the problem solution will be governed by the length scale of the bearing. Thus, it is interesting to compute the difference between the results of the average friction force F^I and hydrodynamic lift $L(t)$ extracted from the fully deterministic simulations F^I_{untext} and L_{untext}, computed neglecting the surface roughness ($h_L(x_1, x_2, t) \equiv 0$):

$$e^{F^I}_{untext} = \frac{F^I_{untext} - F^I}{F^I}, \tag{38}$$

$$e^{L}_{untext} = \frac{L_{untext} - L}{L}. \tag{39}$$

This is shown in Table 5. For $Z=0.5$, $e^{F^I}_{untext}$ is above 10% and as high as 30%. However, for $Z \geq 2.0$ the errors in friction are lower or equal to 7%. The latter results are remarkable due to the low errors attained and to the fact that a computationally inexpensive problem is being solved instead of a complex measured-surface simulation. However, the results for the hydrodynamic lift error $e_{untext}{}^{L}$ are more ambiguous. For $R=8$ and $Z \leq 2.0$ they are lower than 3% and fast decreasing with Z. For the lower curvature pad, the errors for $Z=4$ are higher than 8%, which is considerable. This was already pointed out by Bouassida [11] while comparing results of deterministic simulations of various honed surfaces with one-dimensional untextured-runner simulations.

5. Conclusions

In this work we have discussed two important issues in lubrication analysis: (i) models for the friction force for non-planar surfaces, and (ii) high-resolution simulations of measured surfaces.

The first issue was addressed by direct comparisons of lubrication models with two-dimensional Navier–Stokes results (inertia and cavitation effects were neglected). It was found that the

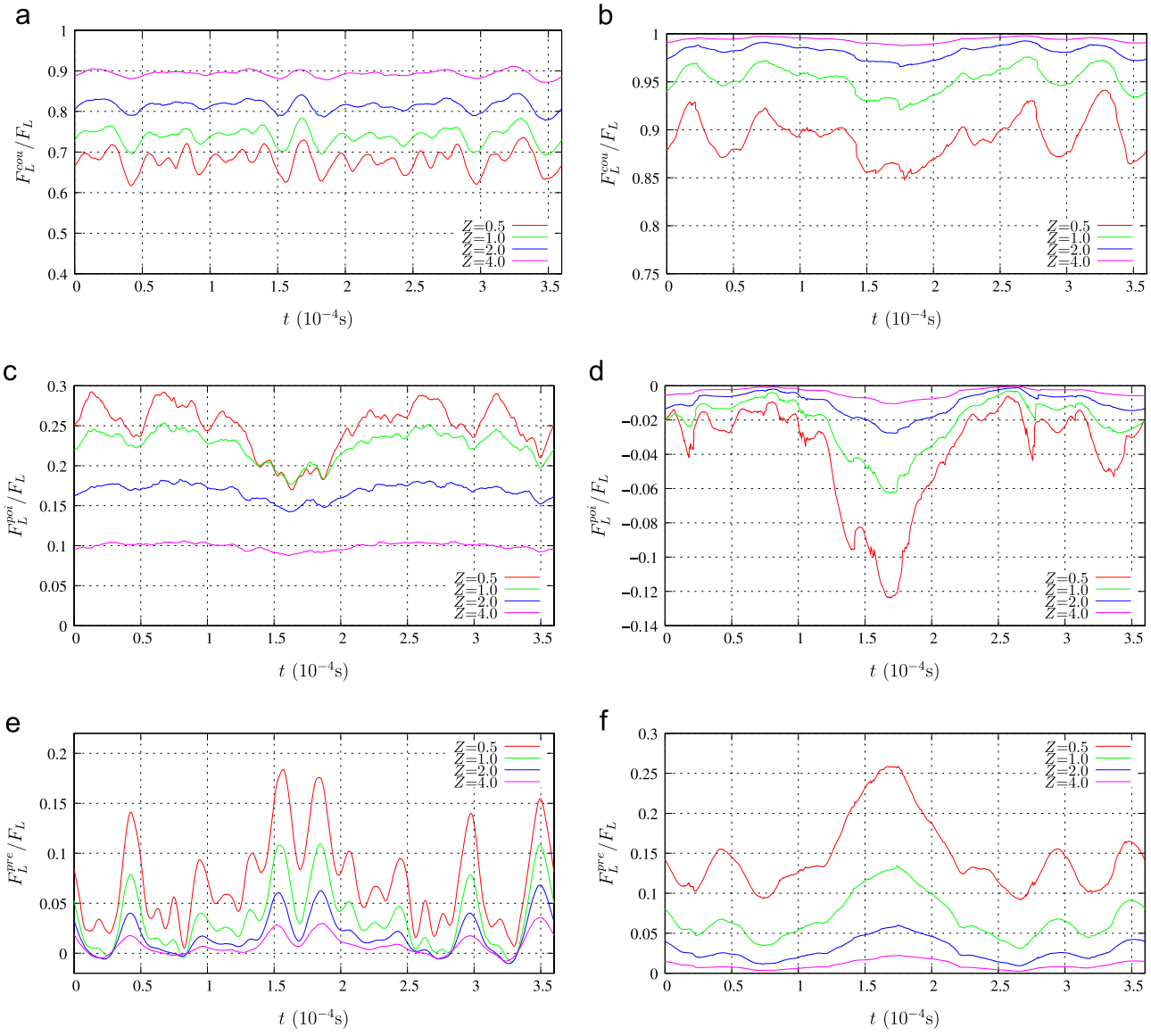

Fig. 9. Friction force terms F_L^{cou}, F_L^{poi} and F_L^{pre} relative to the friction force F_L for strip S_1, $R=8$ (figures (a), (c), (e)) and $R=128$ (figures (b), (d), (f)).

Table 4
Percentage errors e^{II} and e^{III}, averaged in time over a passing of the honed runner.

Strip	Z	% e^{II} ($R=8$)	%e^{II} ($R=128$)	% e^{III} ($R=8$)	% e^{III} ($R=128$)
S_1	4.0	1.1	0.72	10.97	0.7
	2.0	1.8	3.1	18.6	1.9
	1.0	3.4	6.8	26.2	4.7
	0.5	7.2	14.6	32.2	10.8
S_2	4.0	0.43	0.60	10.6	0.42
	2.0	1.2	1.9	18.6	1.5
	1.0	2.0	5.2	26.1	4.1
	0.5	6.2	12.6	32.3	10.3
S_3	4.0	1.1	0.7	10.8	0.7
	2.0	1.2	1.9	19.0	1.5
	1.0	2.4	4.8	26.0	3.9
	0.5	5.6	11.6	32.2	9.9

three-term formulas (16a) and (16b) are the most accurate ones, providing a reasonable estimate of the hydrodynamic friction of rough surfaces at sub-micron clearances, even when the lubrication hypotheses (5) are not being met.

Table 5
Percentage errors $e_{untext}^{F_l}$ and $e_{untext}{}^{L}$ committed by neglecting the surface roughness.

Strip	R	$e_{untext}^{F_l}$ (%)				$e_{untext}{}^{L}$ (%)			
		$Z=0.5$	1.0	2.0	4.0	0.5	1.0	2.0	4.0
S_1	8	−10.5	−4.7	−2.3	−1.2	−5.6	−1.3	−0.1	0.1
	128	−23.1	−12.4	−5.3	1.1	−10.1	−3.5	−4.4	−8.0
S_2	8	−11.2	−5.0	−2.3	−1.2	−8.4	−3.5	−1.7	−0.9
	128	−23.9	−13.1	−6.0	0.2	−20.0	−11.9	−9.0	−8.6
S_3	8	−11.5	−5.33	−2.9	−1.3	−9.3	−4.2	−2.1	−1.2
	128	−24.3	−13.4	−6.4	−0.16	−21.4	−12.9	−9.4	−8.5

Regarding the second issue, simulations of a measured honed surface were reported using the conservative time-dependent Elrod–Adams model with spatial resolutions as fine as 0.25 μm per cell (4000 × 800 mesh). This allowed us to confirm the mesh convergence of the numerical method for the challenging topographies of measured data, and suggested cell sizes of a quarter or

even half of the measurement resolution (here 0.5 μm and 1 μm respectively) as a reasonable compromise of accuracy and cost for the simulation of honed runners. It was also seen that for large clearances, good accuracy can be achieved by performing low-cost simulations in which the surface roughness is neglected.

In the measured-surface simulations, the significance of each term of the friction formula (16a) was computed, so as to assess the error introduced by some incomplete models found in the literature. It was observed that, for clearances much larger than the roughness amplitude, the Couette term of the friction force is dominant and can be taken as an acceptable approximation. For high loads (small clearances), only the complete formulas (16a) and (16b) yield accurate results.

Acknowledgements

The authors thank the financial support of this work provided by CAPES (grant PROEX-8434433/D), FAPESP (grants 2011/24147-5 and 2014/19249-1) and CNPq (grant 447904/2014-0).

References

[1] Tzeng ST, Saibel E. Surface roughness effect on slider bearing lubrication. ASLE Trans 1967;10:334–8.
[2] H.Christensen, Stochastic models of hydrodynamic lubrication of rough surfaces, Proc Int Mech Eng 184, 1969, 1013-1026.
[3] Patir N, Cheng. HS. An average flow model for determining effects of three-dimensional roughness on partial hydrodynamic lubrication. Trans ASME 1978;100:12–7.
[4] Patir N, Cheng HS. Application of average flow model to lubrication between rough sliding surfaces. Trans ASME 1979;101:220–9.
[5] Elrod HG. A general theory for laminar lubrication with Reynolds roughness. Trans ASME 1979;101:8–14.
[6] Bayada G, Chambat M, Faure JB. Some effects of the boundary roughness in a thin film boundary control and boundary variations. Lect Notes Comp Sci 1988;100:96–115.
[7] Bayada G, Chambat M, Faure JB, Double A. Scale analysis approach of the Reynolds roughness. Comments and application to the journal bearing. ASME J Tribol 1989;111:323–30.
[8] Jai M. Homogenization and two-scale convergence of the compressible Reynolds lubrication equation modeling the flying characteristics of a rough magnetic head over a rough rigid-disk surface. Math Model Numer Anal 1995;29:199–233.
[9] Buscaglia G, Ciuperca I, Jai M. Homogenization of the transient Reynolds equation. Asymptot Anal 2002;32:131–52.
[10] G.Buscaglia and M.Jai, Homogenization of the generalized reynolds Reynolds equation for ultra-thin gas films and its resolution by FEM, ASME Tribol 126, 2004, 547-552.
[11] Bouassida H. Lubricated piston ring cylinder liner contact: influence of the liner microgeometry [PhD thesis]. INSA de Lyon; 2014.
[12] Mezghani S, Demirci I, Zahouani H, El Mansori M. The effect of groove texture patterns on piston-ring pack friction. Precis Eng 2012;36:210–7.
[13] Mezghani S, Demirci I, Yousfi M, El Mansori M. Mutual influence of crosshatch angle and superficial roughness of honed surfaces on friction in ring-pack tribo-system. Tribol Int 2013;66:54–9.
[14] Caciu C, Decencière E. Numerical analysis of a 3D hydrodynamic contact. Int J Numer Methods Fluids 2006;51:1355–77.
[15] Checo H, Ausas R, Jai M, Cadalen J-P, Choukroun F, Buscaglia G. Moving textures: simulation of a ring sliding on a textured liner. Tribol Int 2014;72:131–42.
[16] H.Checo, A.Jaramillo, M.Jai and G.Buscaglia, Texture-induced cavitation bubbles and friction reduction in the Elrod-Adams model, Proc IMechE Part J Eng Tribol 229, 2015, 478-492.
[17] Medina S, Fowell M, Vladescu S, Reddyhoff T, Pegg I, Olver A .et al., Transient effects on lubricated textured bearings, Proc IMechE Part J Eng Tribol 229, 2015, 523-537.
[18] A.Ronen, I.Etsion and Y.Kligerman, Friction-reducing surface-texturing in reciprocating automotive components, Tribol Trans 44, 2001, 359-366.
[19] Etsion I, Kligerman Y, Shinkarenko A. Improving tribological performance of piston rings by partial surface texturing. J Tribol 2005;127(3):632–8.
[20] Shinkarenko A, Kligerman Y, Etsion I. The effect of surface texturing in soft elasto-hydrodynamic lubrication. Tribol Int 2009;42:284–92.
[21] Ramesh Ashwin, Akram Wasim, Mishra Surya P, Cannon Andrew H, Polycarpou Andreas A, King William P. Friction characteristics of microtextured surfaces under mixed and hydrodynamic lubrication. Tribol Int 2013;57:170–6.
[22] Y.Kligerman and A.Shinkarenko, Analysis of friction in surface textured components of reciprocating mechanism, Proc IMechE Part J Eng Tribol 229, 2014, 336-349.
[23] Profito F, Tomanik E, Zachariadis D. Effect of cylinder liner wear on the mixed lubrication regime of TLOCRs. Tribol Int 2015;93:723–32.
[24] Akchurin A, Bosman R, Lugt P, van Drogen M. On a model for the prediction of the friction coefficient in mixed lubrication based on a load-sharing concept with measured surface roughness. Tribol Lett 2015;59:19.
[25] Ausas R, Ragot P, Leiva J, Jai G, Bayada M, Buscaglia G. The impact of the cavitation model in the analysis of micro-textured lubricated journal bearings. ASME J Tribol 2009;129:868–75.
[26] Elrod HG, Adams M. A computer program for cavitation. Technical report 190, 1st LEEDS LYON Symposium on Cavitation and Related Phenomena in Lubrication, I.M.E. 103:354; 1974.
[27] Frêne J. Hydrodynamic lubrication: bearings and thrust bearings. Tribol Interface Eng Ser. Elsevier; 1997.
[28] Bayada G, Chambat M. The transition between the Stokes equations and the Reynolds equation: a mathematical proof. Appl Math Optim 1986;14(1):73–93.
[29] Ausas R, Jai M, Buscaglia G. A mass-conserving algorithm for dynamical lubrication problems with cavitation. ASME J Tribol 2009;131:031702: 7 p.
[30] Venner CH, Lubrecht AA. Multilevel methods in lubrication. Amsterdam, The Netherlands: Elsevier; 2000.
[31] van Odyck D, Venner C. Stokes flow in thin films. ASME J Tribol 2003;125:121–34.
[32] Almqvist T, Larsson R. Some remarks on the validity of Reynolds equations in the modeling of lubricant film flows on the surface roughness scale. ASME J Tribol 2004;126:703–10.
[33] G.C.Buscaglia and R.F.Ausas, Variational formulations for surface tension, capillarity and wetting, Comput Methods Appl Mech Eng 200, 2011, 3011-3025.
[34] Ausas R, Sousa F, Buscaglia G. An improved finite element space for discontinuous pressures. Comput Methods Appl Mech Eng 2010;199:1019–31.
[35] R.Codina, J.Blasco, G.Buscaglia and A.Huerta, Implementation of a stabilized finite element formulation for the incompressible Navier–Stokes equations based on a pressure gradient projection, Int J Numer Methods Fluids 37, 2001, 419-444.
[36] E. Abbott and F. Firestone, Specifying surface quality —a method based on accurate measurements and comparison, J Mech Eng 55, 1933, 569-572.